A Global Sensitivity-Based Identification of Key Factors on Stability of Power Grid with Multi-Outfeed HVDC

Li Shen, Li Jiang, Qiao Ming*, Qing Wang, and Yiyu Wen

***Abstract*—Multi-outfeed configuration of high voltage direct current (HVDC) links is being increasingly developed in China's power source grids. Although CIGRE has provided many indices for assessing the security of asynchronous interconnected power grids, massive stochastic renewables significantly induce challenges for dispatchers in determining how numerous operational variables affect these indices, such that it can be difficult to plan a power grid that well bears multi-outfeed HVDCs. To solve this problem, an index integration-combined global sensitivity analysis (GSA) method is proposed. First, several indices that quantify voltage stability, frequency stability, and transient stability are provided. These indices are then fused by the proposed entropy weight-fuzzy analytic hierarchy process (EWF-AHP) method, such that the original massive indices are reduced to only one. Finally, a Gaussian process-based GSA method is applied to analyze the sensitivity of the syncretic index versus the uncertainty variables. The collected sensitivity information can further inform the planning strategies for multi-HVDC outfeed power grids. A real-world case in Southwest China proved the effectiveness of the proposed framework, and implied the potential of the method for tuning or planning operational modes.**

***Index Terms*—Analytic hierarchy process, Gaussian process, global sensitivity analysis, multi-outfeed HVDC, stability index.**

I. Introduction

Due to the geographic divergence of energy in China, the development of China's power grid is continually turning into high-capacity and long-distance HVDC transmission [1]. Renewable energy resources and flexible demand assets are being proliferated in power systems to enhance energy sustainability and efficiency [2]. The uncertainty of renewable energy affects the reliable operation of power system [3]. In order to realize transregional power utilization from rich clean energy in Southwest China to load centers in East China, Southwest power grid made great efforts to develop multi-outfeed ultra-HVDC power system [4], [5]. Multi-outfeed HVDC power system is made up of two or more DC lines with relatively close electrical distances and the fed AC power grid. In such a system, the rectifier stations of the multi-circuit DC system are concentrated in the same region, and there is close coupling between the rectifier stations. Up to now, several asynchronous HVDC lines that connect the Southwest power grid and the East China power grid have been put into operation successively [6]. Based on this fact, as the sending-end power grid, the operating patterns of the Southwest power grid have changed a lot, e.g., the contradiction between the strong DC outfeed and the weak AC grid [7]. The current sending-end power grid operational practice shows that the system faults easily trend to produce a cascading failure, which threatens the safety of both sides of HVDC links. As a result, it is significant to develop intact sets of indices for multi-outfeed power grids in order to understand operational conditions and plan more reliable operating patterns.

At present, there have been studies on the security assessment of asynchronous HVDC systems. Yet, the most efforts can only be found in multi-infeed HVDC (MIDC) systems. For instance, an on-line power/voltage stability index for MIDC has been proposed in [8], but it is not proven to be applicable in multi-outfeed systems. The load margin index in [9] can effectively evaluate the static voltage stability of the power grid. In [10], a control strategy based on the sensitivity index of the singular value of the Jacobian matrix is proposed to increase the stability of the AC/DC system. But the physical significance of the sensitivity index is not clear. Considering inter-inverter interactions, a multi-infeed voltage interaction factor index is proposed for the voltage stability evaluation of MIDC [11]. In [12], two generic indices, i.e., the multi-infeed effective short-circuit ratio and the multi-infeed interaction factor, for linking power grid structural strength and operational stability of multi-outfeed HVDC systems were proposed. The maximum available power (MAP) has been investigated in [13], it enables aware of stability margin for HVDC. In [1], the effect of transmission capacity of multi-outfeed HVDC system on transient voltage stability was analyzed, and attained quantitative evaluation indices. Although many independent indices have been carried out, one trouble for dispatchers is that one can be quite exhausting to catch the trends of these indices themselves, which are vital for dispatching or planning tasks. The other obstacle comes from the truth that, current research still lacks a holistic perspective to figure out exactly how the critical operational variables or their combinations will affect the existing indices. In this regard, controlling or optimizing the massive indices via power system planning or operating can be a burdensome task, especially in an environment full of uncertainties.

Many researchers noticed the above issues and proposed a novel solution, namely sensitivity analysis (SA). Generally, two

This paper was submitted for review on March 13, 2023.This work is supported by the science and technology project of State Grid Southwest Branch Corporation (SGSW0000FGJS2310063).

Li Shen, Li Jiang, Qing Wang, and Yiyu Wen is with the State Grid Southwest Branch Corporation, State Grid Corporation of China, Chengdu, Sichuan (e-mail: slklillua@163.com; 375310472@qq.com; 464615873@qq.com; 287618178@qq.com).

Qiao Ming* is studying at the Colledge of Electric Engineering, Sichuan University, Chengdu, China (e-mail: 2643741059@qq.com).

categories can be declared, i.e., local SA (LSA) and global SA (GSA) [14]. LSA intends to derive how a variable shift will change a concerned response in the vicinity of a specified operational condition. It greatly adapts to conduct stepwise control [15], however, can be incomplete sight to clarify the dominated factors in a system. In light of this, GSA becomes necessary. It can provide more integrated information about the global relationship between operations and the concerned indices by establishing sensitivity to covering the entire feasible region [16]. Back to our task, GSA can strip down all weak-related inputs from such a tremendous operational region of multi-outfeed HVDC systems, and precisely expose the most leading inputs for further planning or operating. Nevertheless, in our concerned task, GSA can still undergo computational burden from traversing all indices.

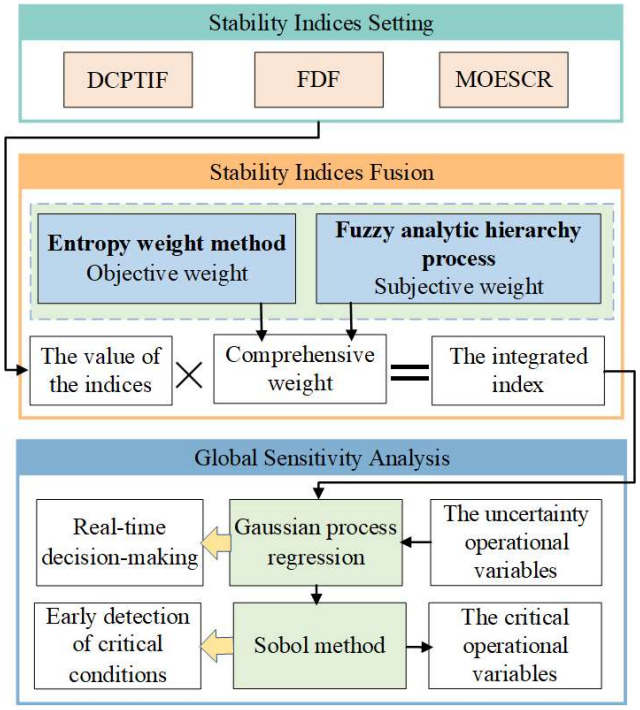

Fig. 1. The technical roadmap.

Therefore, to fix the above problems, this paper provides two major ideas shown as follows, which are also our contributions:

a) We involved several indices (e.g., multi-outfeed effective short circuit ratio, frequency deviation factor, and DC power transfer impact factor) for comprehensively quantifying voltage stability, frequency stability, and transient stability in a multi-outfeed HVDC system. To further allow dispatchers to explicitly master the operating conditions, an entropy weight fuzzy analytic hierarchy process (EWF-AHP) is proposed. This method intends to reduce the dimensionality of the mentioned indices, and draw the sending-end operational patterns with only a few compound indices.

b) A Sobol's GSA method is adopted to help dispatchers deeply understand how operational variables affect the provided indices. It is notable that the Sobol method can be time-consuming for our task, because of some indices may ask for laborious iterative computation or time-domain simulations. To conquer this cumber, Gaussian process is introduced to enhance Sobol. It significantly accelerates index calculations via its parameterized random process and modelled stochastic variables.

The overall technical roadmap of the paper is shown in Fig. 1. First, establish indices layer with indices DCPTIF, FDF, and MOESCR. Then, calculate their fusion weights by using EWF-AHP, and obtain the integrated index value. Finally, use uncertainty operational variables as inputs and the integrated index as the objective function to construct a GPR model. Based on the GPR model, analyze the global sensitivity using the Sobol method and output the key operational variables that affect the integrated index. The GPR module can be used for real-time decision-making, while the Sobol module can be used for early detection of critical conditions.

The remainder of this paper is organized as follows: In Section II, the indices for evaluating multi-outfeed HVDC systems are introduced. In Section III, basic principle of reducing multiple indices via EWF-AHP is introduced. In Section IV, on the application scenarios of multi-outfeed HVDC system, Sobol GSA improved with Gaussian process surrogate is advanced. The proposed method is verified in the Southwest China power grid in Section V. Section VI concludes the paper.

II. The Applied Indices For Evaluating Stability of Multi-Outfeed HVDC Systems

Existing studies render copious indices for evaluating the stability of multi-outfeed HVDC systems, mainly focusing on establishing nexus between HVDC transmission lines and AC-side power grid structure. To cover key concerned stability issues of dispatchers in multi-outfeed HVDC systems, which are transient stability, voltage stability, and frequency stability, this paper introduced three highly related indices, i.e., DC power transfer impact factor (DCPTIF), multi-outfeed effective short-circuit ratio (MOESCR), and frequency deviation factor (FDF). These indices measure AC/DC hybrid system security with only steady variables or parameters.

A. Transient Stability Index

To enable generalized dispatch tasks such as unit commitment and economic dispatch, transient stability constraints of AC systems are usually mapped into several power flow limits of several critical AC power transfer corridors. Follow this truth, a tricky alternative to measure transient stability of AC/DC systems is to figure out how much power will retransfer from DC out-feeders to the critical AC inter-corridors if commutation failures or blockings occur at HVDC lines. Thus, DCPTIF is proposed. It is an index for quantifying the strength of AC systems sustaining outfeed HVDC lines with regard to transient stability. The DCPTIF index for each AC line can be described as:

$$F_{DCPTIF} = \frac{\Delta P_{DCT} \times P_{ac} \times c}{S_{ac} \times P_{ac-max}} \tag{1}$$

where F_{DCPTIF} is the DCPTIF index, ΔP_{DCT} is the power transfer from HVDC to AC inter-corridors after HVDC blocking, S_{ac} is the short circuit capacity on both sides of each

AC line, P_{ac} is the actual transmission power of the AC line, P_{ac-max} is the power transfer limit for the AC line, c is the amplification factor introduced to facilitate result identification.

The DCPTIF index intends to depict an acknowledged phenomenon that, when disturbances occur in some outfeed HVDC lines, it is inevitable that a certain capacity of DC power will be retransferred to adjacent AC system power grid, affecting transient stability of the AC power grid. In this paper, we use DCPTIF to measure the transient stability of multi-outfeed HVDC power grids.

B. Voltage Stability Index

In the CIGRE Conference, the multi-infeed effective short circuit ratio (MIESCR) index is proposed to evaluate the voltage support strength of AC system to multiple HVDC lines [17].

MIESCR of the *i*-th converter can be described as follows:

$$I_{MIESCRi} = \frac{S_{ci} - Q_{cNi}}{P_{dNi} + \sum_{j=1,j\neq i} I_{MIIFji} P_{dNj}} \tag{2}$$

where S_{ci} is the three phase short-circuit capacity at AC bus connecting the *i*-th converter, P_{dNi} is rated power of the *i*-th HVDC line, Q_{cNi} is the reactive power provided by AC filter and shunt capacitor in converter station when the voltage AC bus coupling the *i*-th converter station is rated, I_{MIIFji} is the multi-infeed interaction factor of the *i*-th converter w.r.t. the *j*-th converter, which can be estimated by perturbation simulation, as given below:

$$I_{MIIFji} = \frac{\Delta U_j}{\Delta U_i} \tag{3}$$

where ΔU_i is the voltage disturbance of AC bus connecting the *i*-th converter station, about 1% in general. ΔU_j is the voltage variation of AC bus connecting the *j*-th converter station.

At present, MIESCR has been widely recognized and used [18], [19]. MIESCR is also proven to be applicable for multi-outfeed HVDC systems, which is known as multi-outfeed interaction factor (MOIF) and multi-outfeed effective short-circuit ratio (MOESCR) [20]. The calculation process of MOIF and MOESCR are highly consistent with MIIF and MIESCR. The difference is that MOIF and MOESCR conduct computation on rectifier side of HVDC lines, instead of inverter side.

C. Frequency Stability Index

Once HVDC lines are largely disturbed by commutation failure or DC blocking, tremendous imbalanced power will inject into the adjacent AC power grid, including sending-end and receiving-end. The large power disturbance can cause severe issue in frequency stability of AC power grid. Earlier works show that frequency deviation factor (FDF) can be used for quantifying frequency supporting strength of AC power grid [21]. This index is also workable for our case, thus it is introduced in this paper. FDF index is defined as:

$$\beta = \frac{1}{R_{eq}} + D_{eq} \tag{4}$$

where R_{eq} is the equivalent speed change rate for all generators, D_{eq} is the equivalent frequency regulation factor of active loads. The two variables depend on unit commitment and load configuration, which are calculated by using (5) and (6).

$$\frac{1}{R_{eq}} = \sum_i \frac{1}{R_i} \frac{P_{gNi}}{f_N} \tag{5}$$

where $P_{\mathrm{gN}i}$ is the rated power of the *i*-th generator, f_{N} is the system rated frequency and $R_i = (\omega_{\mathrm{NL}} - \omega_{\mathrm{FL}})/\omega_0 \times 100\%$ is speed change rate of the *i*-th generator, ω_{NL} is the no-load static speed, ω_{FL} is the full-load static speed, ω_0 is the rated speed. The active load frequency regulation factor D_{eq} is computed by using (6).

$$D_{eq} = \frac{\Delta P_L}{\Delta f} \tag{6}$$

where ΔP_{L} is the overall active load variation, Δf is the frequency variation.

Consequently, three indices are introduced to build the basic index set in this paper. Interestingly, some of these indices are quite hard to obtain. For example, the D_{eq} in (4) is highly dependent on load configuration in a power grid. It can only be estimated based on power system simulator and historical operational data. Another instance is that the Q_{cNi} in (2) usually must be operated following some engineering rules. Under such circumstance, the mentioned indices can be troublesome to be acquired. Mastering these indices over the operational region in a realistic large multi-outfeed HVDC is thus pretty laborious for dispatchers.

III. Entropy Weight-Fuzzy Analytic Hierarchy Process-Based Index Set Reduction

As mentioned before, dispatchers face challenges to precisely and simultaneously master multiple indices. This section introduces an index integration method to reduce these indices into few ones, such that dispatchers only need to take care of few principal information, which improves efficiency in planning or dispatching a sending-end grid. The method is carried out upon traditional analytical hierarchy process (AHP). However, AHP is difficult to ensure the consistency of the evaluation process, and can be inaccurate in integrating multiple indices. Therefore, an entropy weight-fuzzy analytic hierarchy process (EWF-AHP) is proposed to lessen the impact of experts' subjective preferences and decrease reliance on original data [22].

EWF-AHP first calculates the subjective weight using the fuzzy analytic hierarchy process, and then it calculates the objective weight using the entropy weight method. The comprehensive weight is derived after taking each index's own variation degree into account. The following are the precise steps for implementation:

1) Calculate subjective weights and check consistency. Apply the fuzzy analytic hierarchy process, form a fuzzy complementary judgment matrix $\boldsymbol{A}$ according to expert opinions:

$$\boldsymbol{A}=\begin{pmatrix} a_{11} & \cdots & a_{1n} \\ \vdots & \ddots & \vdots \\ a_{n1} & \cdots & a_{nn} \end{pmatrix}_{n\times n} \tag{7}$$

where n is the number of indices, specifically referring to the three applied indices MOESCR, FDF and DCPTIF. The a_{ij} represents the importance level of indicator i relative to indicator j, $a_{ii}=1$, $a_{ji}=1/a_{ij}$. Using the 1-9 Scale method [23], experts can compare the indices of the same level pairwise based on subjective opinions to obtain $\boldsymbol{A}$. The 1-9 Scale method is shown in Table I.

TABLE I
THE 1-9 SCALE METHOD

Scale of a_{ij}	Meaning
1	Element *i* is as important as *j*
3	Element *i* is slightly more important than *j*
5	Element *i* is obviously more important than *j*
7	Element *i* is stronger than *j*
9	Element *i* is extremely important than *j*
2, 4, 6, 8	The median of the above two adjacent judgments
reciprocal	$a_{ji}=1/a_{ij}$

If the experts' comparisons of the n indices are absolutely objective, that is, $a_{ij}\times a_{jx}=a_{ix}$, then the matrix $\boldsymbol{A}$ has consistency. If $\boldsymbol{A}$ is consistent, the normalized form of the positive eigenvector corresponding to its maximum positive eigenvalue represents the weight vector of each index.

The maximum positive eigenvalue of $\boldsymbol{A}$ and its corresponding eigenvector are denoted as λ_{max} and $\overline{\boldsymbol{w}}$, $\overline{\boldsymbol{w}}=(\overline{w}_1,\overline{w}_2,\cdots,\overline{w}_n)^T$. Normalize the vector according to $w_i=\overline{w}_i/\sum_{i=1}^{n}\overline{w}_i$, obtain the subjective weight $\boldsymbol{W}$:

$$\boldsymbol{W}=(w_1,w_2,\cdots,w_n)^T \tag{8}$$

Then, check the consistency of judgment matrix $\boldsymbol{A}$:

$$C_I=\frac{\lambda_{max}-n}{n-1} \tag{9}$$

Generally, if the consistency index $C_I\neq 0$, the consistency ratio C_R will be calculated to check the consistency.

$$C_R=\frac{C_I}{R_I} \tag{10}$$

where R_I is the average random consistency indicator. When $C_R<0.1$, it is considered that the judgment matrix $\boldsymbol{A}$ has satisfactory consistency; otherwise, it is essential to readjust the value of the judgment matrix and repeat the above stages until the consistency test is satisfied.

2) Calculate objective weights. Considering the correlation between the actual sample data, the entropy weight method is introduced. Establish the original data matrix $\boldsymbol{X}$ based on the indicator data.

$$\boldsymbol{X}=\begin{pmatrix} x_{11} & \cdots & x_{1n} \\ \vdots & \ddots & \vdots \\ x_{m1} & \cdots & x_{mn} \end{pmatrix}_{m\times n} \tag{11}$$

where m is the number of data samples and n is the number of indices.

To eliminate the error caused by different measurement range and value interval of all indicators, we must make sure that all data are processed in a dimensionless manner. For positive indices and negative indices, min-max standardization (MMS) is adopted.

For positive indices

$$v_{ij}=\frac{x_{ij}-\min(x_i)}{\max(x_i)-\min(x_i)} \tag{12}$$

For negative indices

$$v_{ij}=\frac{\max(x_i)-x_{ij}}{\max(x_i)-\min(x_i)} \tag{13}$$

where v_{ij} is the value of each indicator data standardized, x_i is the given indicators.

The objective weight $\boldsymbol{H}$ is calculated by using (14)-(17)

$$p_{ij}=\frac{v_{ij}}{\sum_{i=1}^{m}v_{ij}} \tag{14}$$

$$e_j=-\frac{1}{ln\,m}\sum_{i=1}^{m}p_{ij}\ln(p_{ij}) \tag{15}$$

$$h_j=\frac{(1-e_j)}{\sum_{j=1}^{n}(1-e_j)} \tag{16}$$

$$\boldsymbol{H}=(h_1,h_2,\ldots,h_n) \tag{17}$$

where $i=1,2,\cdots,m$, $j=1,2,\cdots,n$, p_{ij} is the normalized data of the *j*-th index of sample *i*, e_j is the *j*-th index's entropy, h_j is its objective weight.

3) Calculate the comprehensive weight. The combined weight of $\boldsymbol{W}$ and $\boldsymbol{H}$ is calculated and normalized to obtain the comprehensive weight $\boldsymbol{F}$.

$$f_j=\frac{w_jh_j}{\sum_{j=1}^{n}w_jh_j} \tag{18}$$

$$\boldsymbol{F}=(f_1,f_2,\ldots,f_n) \tag{19}$$

where f_j is the comprehensive weight of the *j*-th index.

IV. GAUSSIAN PROCESS REGRESSION-BASED GLOBAL SENSITIVITY ANALYSIS FOR CRITICAL FACTOR IDENTIFICATION IN MULTI-OUTFEED HVDC SYSTEM

Although EWF-AHP has reduced the dimensionality of the applied indices, the well-integrated indices after EWF-AHP are not intuitive enough for help operating or planning tasks. Dispatchers prefer to know what exactly the variables in a sending-end system impact stability of the power grid. Towards this end, a Gaussian process regression (GPR)-based GSA is presented. GPR works for parameterizing operational patterns, then it forwards to realize efficient GSA, such that computationally-intensive physical simulation can be circumvented.

A. Equations of Gaussian Process Regression for Capturing Operational Patterns

Gaussian process regression (GPR) is a non-parametric machine learning algorithm for regression analysis of data based on a Bayesian framework, which is used to deal with the problem of small samples, high dimension and linear inseparability [24]. The Gaussian process function $f(x)$ can be expressed as:

$$f(x) = GP\big(m(x), k(x,x')\big) \tag{20}$$

where, $m(x)$ is the mean value function, $k(x,x')$ is the covariance kernel, x and x' are the value of the two predictive variables. In general, data is preprocessed to make the mean value zero.

Consider a model:

$$y = f(x) + \varepsilon \tag{21}$$

$$\varepsilon \sim N(0, \sigma_n^2) \tag{22}$$

where x is the input vector of observed value, ε is the noise, σ_n^2 is the standard deviation. In our task, x particularly refers to the generator output and load in different regions, and y is the integrated index.

We can get the prior distribution of the observed value y and the joint prior distribution of the observed value y and the predictive value f_*.

$$y \sim N(0, K(X,X) + \sigma_n^2 I_n) \tag{23}$$

$$\begin{bmatrix} y \\ f_* \end{bmatrix} \sim N\left(0, \begin{bmatrix} K(X,X) + \sigma_n^2 I_n & K(X,x_*) \\ K(x_*,X) & K(x_*,x_*) \end{bmatrix}\right) \tag{24}$$

where x_* is test point, $K(X,X) = K_n = (k_{ij})$, I_n is n-order identity matrix. $K(X,x_*) = K(x_*,X)^T$ represent covariance matrix of X and x_*.

Therefore, we can get the posterior distribution of f_*:

$$f_* \,\big|\, X, y, x_* \sim N\big(\overline{f_*}, cov(f_*)\big) \tag{25}$$

where

$$\overline{f_*} = K(x_*,X)[K(X,X) + \sigma_n^2 I_n]^{-1} y \tag{26}$$

$$cov(f_*) = K(x_*,x_*) - K(x_*,X) \times [K(X,X) + \sigma_n^2 I_n]^{-1} K(X,x_*) \tag{27}$$

The mean value $\widehat{u_*}$ and the covariance $\widehat{\sigma_*^2}$ of f_* are as follows:

$$\begin{cases} \widehat{u_*} = \overline{f_*} \\ \widehat{\sigma_*^2} = cov(f_*) \end{cases} \tag{28}$$

Assuming covariance function has square exponential covariance:

$$k(x,x') = \sigma_f^2 \, exp\big(-\frac{1}{2}\big(x - x'^{)^T M^{-1}} (x - x')\big) \tag{29}$$

where $M = diag(l^2)$, l is the variance measure, σ_f^2 is the signal variance.

Establishing negative logarithmic likelihood function $L(\theta)$ for conditional probability of training samples, and then we can obtain the optimal solution of the hyperparameter $\theta = \{M, \sigma_f^2, \sigma_n^2\}$.

$$L(\theta) = \frac{1}{2} y^T C^{-1} y + \frac{1}{2} log\,|C| + \frac{n}{2} log\,2\pi \tag{30}$$

$$\frac{\partial L(\theta)}{\partial \theta_i} = \frac{1}{2} tr\big((\alpha\alpha^T - C^{-1}) \frac{\partial C}{\partial \theta_i}\big) \tag{31}$$

where

$$\begin{cases} C = K_n + \sigma_n^2 I_n \\ \alpha = (K_n + \sigma_n^2 I_n)^{-1} y = C^{-1} y \end{cases} \tag{32}$$

After obtaining the optimal hyperparameter, the mean value $\widehat{u_*}$ and the covariance $\widehat{\sigma_*^2}$ of f_* corresponding to x_* can be obtained by using (26) and (27).

B. Sobol Method for Critical Factor Identification

Sobol method is a global sensitivity analysis (GSA) method based on the analysis of variance (ANOVA) theory introduced in [25]. Sobol is used to evaluate how one input variable or the interaction of multiple variables affects the relevant outputs.

Consider a feature owning several independent variables $X = [X_1, X_2, \cdots X_k]$ in Ω^k:

$$\Omega^k = (x | 0 \le x_i \le 1; i = 1,2,\cdots,k) \tag{33}$$

Based on the high-dimensional model representation of function, the quadratically integrable function $f(x)$ can be decomposed into the sum of 2^k subfunctions, refer to (34) [26]:

$$f(x) = f_0 + \sum_{i=1}^{k} f_i + \sum_{1 \le i \le j \le k} f_{ij} + \cdots + f_{12\cdots k} \tag{34}$$

where

$$\begin{cases} f_i = f_i(x_i) \\ f_{ij} = f_{ij}(x_i, x_j) \\ f_{12\cdots k} = f_{12\cdots k}(x_1, x_2, \cdots, x_k) \end{cases} \tag{35}$$

Under the condition that

$$\int_0^1 f_{i_1 \cdots i_s} dx_{i_t} = 0 \qquad 1 \le t \le s \tag{36}$$

For $1 \le i_1 < \cdots < i_s \le k$, we have

$$\begin{cases} f_0 = \int_{\Omega^k} f(x) dx \\ f_i = -f_0 + \int_0^1 \cdots \int_0^1 f(x) dx_{\sim i} \\ f_{ij} = -f_0 - f_i - f_j + \int_0^1 \cdots \int_0^1 f(x) dx_{\sim (ij)} \end{cases} \tag{37}$$

where $x_{\sim i}$ represents the set of input variables other than x_i, $x_{\sim (ij)}$ represents the set of input variables other than x_i and x_j.

By integrating the square of factorization equation refer to (34), we can get

$$\int_{\Omega^k} f^2(x)dx - f_0^2 = \sum_{s=1}^{k} \sum_{i_1<\cdots<i_s}^{k} f_{i_1,\cdots,i_s}^2 dx_{i_i\cdots}x_{i_s} \tag{38}$$

Thus, we can get the total variance D and the partial variance $D_{i\cdots j}$ of $f(x)$:

$$\begin{cases} D = \int_{\Omega^k} f^2(x)dx - f_0^2 \\ D_{i\cdots j} = \int f_{i\cdots j}^2 dx_i \cdots x_j \end{cases} \tag{39}$$

Equation (38) becomes

$$D = \sum_{i=1}^{k} D_i + \sum_{1\le i<j\le k} D_{ij} + \cdots + D_{12\cdots k} \tag{40}$$

The sensitivity of the input variable is defined as follows:

$$\begin{cases} S_i = \dfrac{D_i}{D} \\ S_{ij} = \dfrac{D_{ij}}{D} \\ S_{\mathrm{T}i} = S_i + \sum\limits_{j\neq i}^{k} S_{ij} + \cdots + S_{12\cdots k} \end{cases} \tag{41}$$

where S_i is the first-order sensitivity coefficient, which represents the main effect of the individual input variable x_i on the system output; S_{ij} is the second-order sensitivity coefficient, which represents the effect of interaction between input variable x_i and x_j on the system output; $S_{\mathrm{T}i}$ is the total sensitivity coefficient, which represents the joint effect of the input variable x_i and its interaction with other input variables on the system output.

V. Experimental Verification and Results

We testified our method using the actual electrical grid in Southwest China. The heavy loading operating mode in 2020 flood season is specified for the further experimental analysis. We prepare operational data before starting our numerical investigations, and the engineering software PSD-BPA is used to calculate the indices. EWF-AHP is then used to fuse these indices. Simulations in the time domain verifying the fusion-index's efficacy. Finally, we demonstrate the GPR-based GSA methodology to identifying key implications on the stability of the multi-outfeed HVDC system. As a result, we offer significant variables that affect the stability of the testing power grid.

A. Index Calculation

To verify the effectiveness of the three applied indices and catch their relationship with stability, the corresponding data of angular trajectories are simulated and collected on five operating modes. The computation results of the applied indices based on simulated operation data are shown in Table II.

From Table II, in operation mode A, the MOESCR, FDF, and DCPTIF are the largest, whereas the operation mode E is just the opposite. Fig. 2-4 depicts the system's maximum node voltage, maximum frequency, and maximum power angle difference trajectories after bipolar blocking disturbance occurrence in this power grid. According to these figures, we find out that operation mode A is of the better voltage and frequency stability, but the worse transient stability, and on the contrary, operation mode E features the better transient stability but the worse voltage and frequency stability. Together with Table II, this case implies that MOESCR and FDF are positively related to voltage and frequency stability, respectively, and DCPTIF negatively correlates to transient stability. Therefore, when using the entropy weight method to calculate objective weights, MOESCR and FDF are normalized using (12), while DCPTIF is normalized using (13).

TABLE II
Calculation Results of Stability Index

System operation mode	MOESCR	FDF	DCPTIF
A	2.4645	5901.7930	13.1489
B	2.4635	5778.8318	13.0881
C	2.4517	5397.6341	12.9675
D	2.4503	5302.4911	12.9175
E	2.4470	5187.3764	12.6594

B. Index Fusion

1) Subjective Weight: according to the dispatching experience, the indicators are evaluated, and based on four different key focuses, scores are assigned and a pairwise comparison is conducted to obtain the fuzzy judgment matrix **A1-A4**. Consistency is then examined for each matrix, and weights are calculated. The results are shown in Table III.

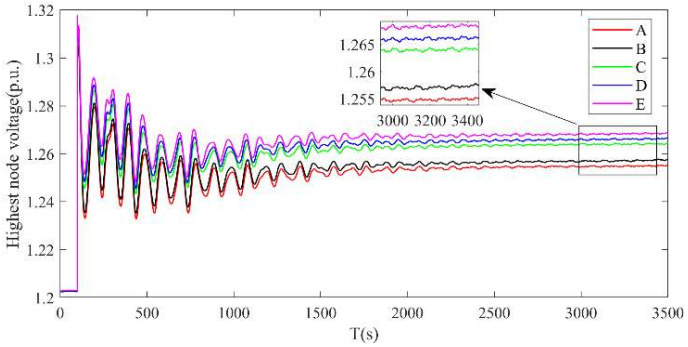

Fig. 2. The highest nodal voltage of the system.

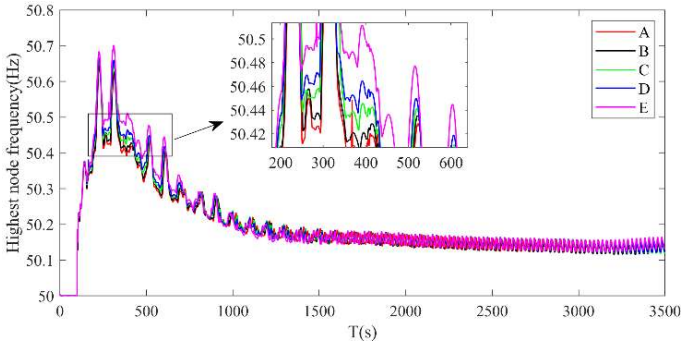

Fig. 3. The highest nodal frequency of the system

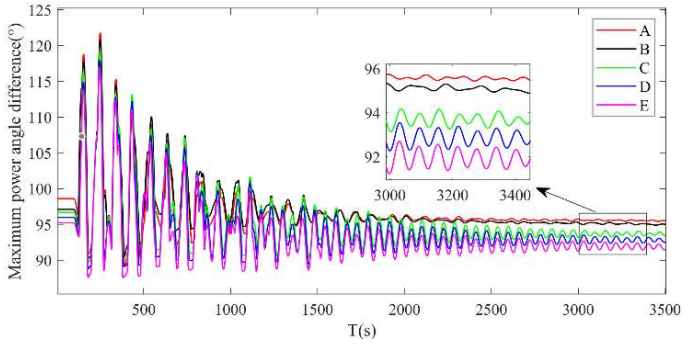

Fig. 4. The maximum power angle difference over synchronous generators.

2) Objective Weight: according to the index data in Section V.A, the objective weights of MOESCR, FDF, and DCPTIF are calculated. The calculation results are 0.2563, 0.3889, and 0.3548.

3) Comprehensive Weight: coupling the subjective and objective weights according to (21). The comprehensive weights of MOESCR, FDF, and DCPTIF are 0.2816, 0.3832, and 0.3351 respectively. As shown in Table III, the subjective weight will be influenced by the preferences of some experts, resulting in a biased weight value. This deviation can be corrected by coupling objective weight and subjective weight. So that the comprehensive weight can fully reflect the concentrated opinions of experts.

TABLE III
CALCULATION RESULTS OF SUBJECTIVE WEIGHTS

Key focus	Weight of MOESCR	Weight of FDF	Weight of DCPTIF
a	0.3069	0.3682	0.3249
b	0.4275	0.3053	0.2672
c	0.2859	0.2834	0.4307
d	0.4307	0.3446	0.2247
Average value	0.3628	0.3254	0.3119

We determine the integrated index values of five power grid operation modes based on the index values and their comprehensive weights. They are in the following numerical order: A, B, E, C, D, with values of 66.4863, 62.4438, 33.5137, 31.2621, and 27.3287, respectively. Operation mode E features the better transient stability but the worse voltage and frequency stability, and the integrated index value under operation mode E is in a middle position. As a result, the value of the integrated index can to some extent reflect the stability of the power system.

Through EWF-AHP, the three indices are fused to form a single integrated index. Using the integrated index, dispatchers can gauge the stability of the present system operation mode. This is helpful for dispatchers to better understand the planning or operating of multi-outfeed HVDC power grids.

C. Global Sensitivity Analysis

If the system's key factors that influence the integrated index's value can be identified, the stability of the system can be increased by adjusting the relevant key variables. We utilize the instance of uncertain generator output and load in various regions, to analyze their global sensitivity to the integrated index. As indicated in Table IV, the instance uses five regions' generator output and load as variables. Set their fluctuation range as per Table V.

TABLE IV
VARIABLES OF GLOBAL SENSITIVITY ANALYSIS

Notation	Connotation	Notation	Connotation
cbG	Generator output in region cb	cbL	Load in region cb
dsG	Generator output in region ds	dsL	Load in region ds
lsG	Generator output in region ls	lsL	Load in region ls
qnG	Generator output in region qn	qnL	Load in region qn
xcG	Generator output in region xc	xcL	Load in region xc

Taking into account the balance between generator output and load, 100 samples are randomly generated. Each sample's MOESCR, FDF, and DCPTIF are calculated, and they are fused into integrated index. These 10 random variables in Table V make up the input of the GSA based on the GPR, in the form of $\boldsymbol{x} = [x_1, \ldots, x_{10}]$. The integrated index value for each random operation mode is the corresponding model response, which has the form $\boldsymbol{y} = [y_1, \ldots, y_{10}]$.

TABLE V
CALCULATION VALUE RANGE OF GENERATOR OUTPUT AND LOAD IN EACH REGION

Variable	Data range	Variable	Data range
cbG	[0, 4840]	cbL	[218.5, 5058.5]
dsG	[4765, 10010]	dsL	[0, 5245]
lsG	[0, 3023.8]	lsL	[569.8,3593.6]
qnG	[366.3, 3260]	qnL	[0, 2893.7]
xcG	[4290.1, 7270]	xcL	[0, 2979.9]

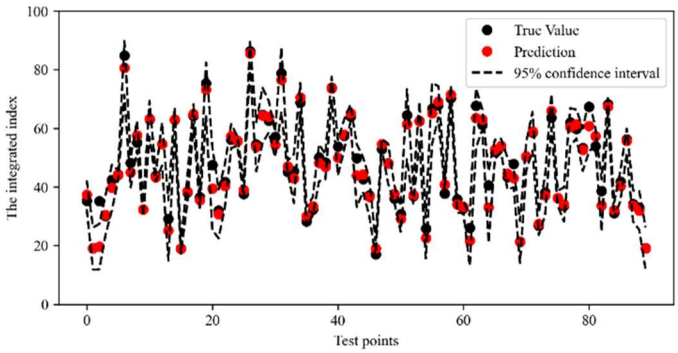

Fig. 5. Gaussian process emulator performance on testing dataset.

The reliability of data-driven method is enhanced by GPR's ability to output the integrated index interval within a certain confidence range. If the integrated index interval of the GPR model is wide, it means that there is a considerable degree of uncertainty in the integrated index value. The integrated index interval inside the GPR's 95% confidence interval is depicted in Fig. 5. It shows that the integrated index interval is narrow. Moreover, the estimated results of the integrated indices obtained by GPR basically maintain a consistent trend with the true values. The performance of the GPR model is quantitatively measured using the mean absolute percentage error (MAPE). The MAPE value over 90 test cases is 4.19%.

This demonstrates that the correlation between these key variables and integrated indicators may be efficiently extracted using GPR.

Next, use the Sobol method for global sensitivity analysis. The first order sensitivity data S_1 and global sensitivity data S_T of each variable to the integrated index are shown in Table VI. Fig. 6 is a sensitivity histogram, which depicts the sensitivity results of the integrated index versus 10 uncertainty variables. S_X in the figure represents the local sensitivity of an uncertainty variable to the integrated index. According to Fig.6, the local sensitivity of each variable is small, and it can not evaluate the impact of the interaction between input variables on the output variables of the model. Therefore, the global sensitivity analysis is essential. The global sensitivity analysis results indicate that, within the range of variables in this paper, variables xcL and lsG have a considerable impact on the integrated indicators, whereas variables lsL, dsG, dsL, cbG, and cbL have a minimal impact and variables qnG, qnL, and xcG have a negligibly weak impact. As a result, the primary variable impacting the value of the integrated index is xcL.

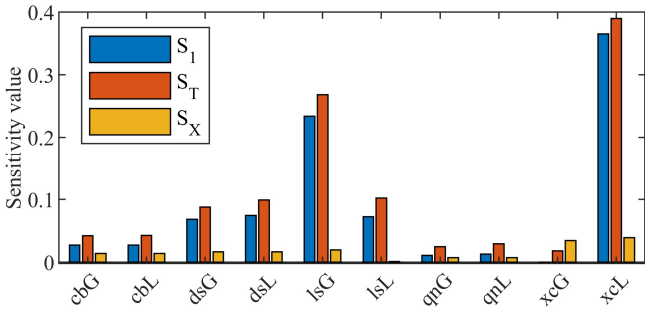

Fig. 6. Sensitivity of the integrated index versus variables.

In addition, Fig. 6 demonstrates that each variable's S_T is greater than S_1. As a result, the integrated index are also impacted by the interactions between variables. Fig. 7 depicts the second order interaction of the variables. There is a significant second order interaction between the load and generator output in the same region. However, all second order interactions are very tiny.

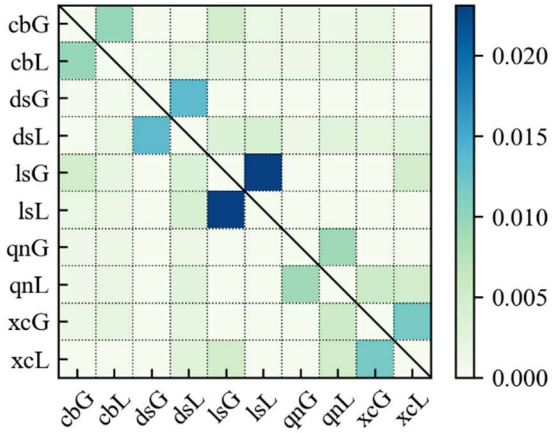

Fig. 7. Second order interaction of variables.

TABLE VI
VARIABLES CALCULATION RESULTS OF S_1 AND S_T

Variable	S_1	S_T	Variable	S_1	S_T
cbG	0.027536	0.042167	cbL	0.027390	0.042478
dsG	0.068213	0.087722	dsL	0.074495	0.099351
lsG	0.233810	0.268257	lsL	0.072424	0.102204
qnG	0.010659	0.024947	qnL	0.013100	0.029247
xcG	-0.001744	0.018260	xcL	0.365337	0.389913

TABLE VII
THE INDEX INTEGRATED BY EWF-AHP

Scheme	Generator output adjustment	Load adjustment	The integrated index
X0(Reference operation mode)	-	-	17.0533
X1	ΔcbG=+1000	ΔcbL=+1000	23.7581
X2	ΔcbG=+2000	ΔcbL=+2000	29.9886
X3	ΔxcG=+1000	ΔxcL=+1000	31.8457
X4	ΔxcG=+2000	ΔxcL=+2000	47.0956

The next work is to verify the effectiveness of the sensitivity results. Taking one operation mode as a benchmark, we adjust the generator output and load of the regions xc and cb, while keeping the generator output and load of the other regions constant. As a result, four comparative operation modes were generated. The calculation results of the integrated index are shown in Table VII. According to Table VII, the integrated index after adjusting region xc is higher than that of adjusting region cb when the adjusted generator output and load are equal. Because the integrated index is more sensitive to the generator output and load in region xc than it is in region cb. Therefore, the sensitivity results obtained by the proposed method are effective. These results demonstrate that the key variables with the biggest effects on the integrated index can be identified utilizing GPR-based GSA. The stability of the system can be enhanced by altering the generator output and load of these regions.

The sample preparation and GPR training took about 16 minutes and 7.69s, respectively. Since these two stages are pre-executed offline (e.g., year ahead or day-ahead), their elapsed times are acceptable. Once the GPR is well settled, it only took 0.93s and 2.35s for evaluating a coming operating condition and early detection of critical conditions, respectively. Evidently, the proposed algorithm hits real time decision demands, and helps dispatchers improve efficiency of look-ahead operating mode analysis.

VI. CONCLUSION

To effectively assess structural strength, as well as help dispatchers with better understanding of planning or operating in multi-outfeed HVDC power grids, an index integration-combined global sensitivity analysis (GSA) method is proposed. Concretely, several basic indices are firstly provided to cover concerned security incidents in multi-outfeed HVDC systems. Then, based on entropy weight-fuzzy analytic hierarchy process (EWF-AHP), primordial multiple indices are reduced into an integrated index, such that

dispatchers can be more comprehensible in planning or operating multi-outfeed HVDC systems. At the end, to allow dispatchers to master planning or operating of sending-end power grids more deeply, a Gaussian process-based GSA is proposed. It specifically uses Gaussian process to parameterize the correlation of operational variables versus the integrated index. The Sobol method is used to figure out the contributions of each concerned component (e.g., operational variable or variable combination) towards the index, and identify the key operational variables. Finally, the stability of the system can be enhanced by adjusting the critical operational variables. The real-world experimental results in the Southwest China power grid justified the effectiveness of the proposed method.

Yet, the proposed method is only testified under a heavy loading operating mode in flood season. The actual operation of the power grid is much more complex and is hard to be characterized through sole seasonal typical operation mode. Under multiple typical operating modes, the uncertainty of operational variables may conflict, potentially canceling each other out or averaging each other. In future works, we will try to precisely identify typical operating modes, then distribute the proposed method on these patterns.

REFERENCES

[1] M. Wang, G. Zhang, and Z. Zhang, "Impact of HVDC transmission capacity on multi-send HVDC system voltage stability," ENERGY REP, vol. 8, pp. 1004-1010, Nov. 2022, 10.1016/j.egyr.2022.05.267.

[2] Y. Liu, L. Wu and J. Li, "A Fast LP-Based Approach for Robust Dynamic Economic Dispatch Problem: A Feasible Region Projection Method," *IEEE Transactions on Power Systems*, vol. 35, no. 5, pp. 4116-4119, Sept. 2020, 10.1109/TPWRS.2020.3004058.

[3] Z. Li, Y. Xu, S. Fang, X. Zheng and X. Feng, "Robust Coordination of a Hybrid AC/DC Multi-Energy Ship Microgrid With Flexible Voyage and Thermal Loads," *IEEE Transactions on Smart Grid*, vol. 11, no. 4, pp. 2782-2793, July 2020, 10.1109/TSG.2020.2964831.

[4] K. Meng, W. Zhang, J. Qiu, Y. Zheng, and Z. Y. Dong, "Offshore Transmission Network Planning for Wind Integration Considering AC and DC Transmission Options," *IEEE Trans. Power Syst.,* vol. 34, no. 6, pp. 4258-4268. Nov. 2019, 10.1109/TPWRS.2019.2912414.

[5] F. Kong, Z. Hao, and B. Zhang, "A Novel Traveling-Wave-Based Main Protection Scheme for ±800 kV UHVDC Bipolar Transmission Lines," *IEEE Trans. Power Del.*, vol. 31, no. 5, pp. 2159-2168. Oct. 2016, 10.1109/TPWRD.2016.2571438.

[6] B. Zhou et al., "Principle and Application of Asynchronous Operation of China Southern Power Grid," *IEEE Trans. Emerg. Sel. Topics Power Electron.*, vol. 6, no. 3, pp. 1032-1040. Sept. 2018, 10.1109/JESTPE.2018.2830409.

[7] H. Zhou, Y. Su, Y. Chen, Q. Ma, and W. Mo, "The China Southern Power Grid: Solutions to Operation Risks and Planning Challenges," *IEEE Power Energy Mag*, vol. 14, no. 4, pp. 72-78. Jul. 2016, 10.1109/MPE.2016.2547283.

[8] J. Xu et al., "An on-line power/voltage stability index for multi-infeed HVDC systems," *J MOD POWER SYST CLE*, vol. 7, no. 5, pp. 1094-1104. Sept. 2019, 10.1007/s40565-019-0507-8.

[9] L. Bai et al., "Confidence interval estimates for loading margin sensitivity for voltage stability monitoring in the presence of renewable energy," *IEEE Power and Energy Society General Meeting (PESGM),* Boston, MA, USA, 2016, pp. 1-5, 10.1109/PESGM.2016.7741802.

[10] O. A. Urquidez and L. Xie, "Singular Value Sensitivity Based Optimal Control of Embedded VSC-HVDC for Steady-State Voltage Stability Enhancement," *IEEE Transactions on Power Systems*, vol. 31, no. 1, pp. 216-225, Jan. 2016, 10.1109/TPWRS.2015.2393253.

[11] H. Xiao and Y. Li, "Multi-Infeed Voltage Interaction Factor: A Unified Measure of Inter-Inverter Interactions in Hybrid Multi-Infeed HVDC Systems," *IEEE Trans. Power Del*., vol. 35, no. 4, pp. 2040-2048. Aug. 2020, 10.1109/TPWRD.2019.2960393.

[12] Z. Xu, Z. Xu, and L. Xiao, "Analysis and assessment standards of power stability of multi-send HVDC systems," *JoE,* vol. 2019, no. 16, pp. 748-753, Mar. 2019, 10.1049/joe.2018.8398.

[13] "IEEE Guide for Planning DC Links Terminating at AC Locations Having Low Short-Circuit Capacities," *IEEE Std 1204-1997*, vol., no., pp.1-216, 21 Jan. 1997, 10.1109/IEEESTD.1997.85949.

[14] B. Sudret, "Global sensitivity analysis using polynomial chaos expansions," *Reliab. Eng. Syst. Saf.*, vol. 93, no. 7, pp. 964-979, Jul. 2008, 10.1016/j.ress.2007.04.002.

[15] F. Ni, M. Nijhuis, P. H. Nguyen, and J. F. G. Cobben, "Variance-Based Global Sensitivity Analysis for Power Systems," *IEEE Trans. Power Syst.*, vol. 33, no. 2, pp. 1670-1682. Mar. 2018, 10.1109/TPWRS.2017.2719046.

[16] K. Ye, J. Zhao, C. Huang, N. Duan, Y. Zhang, and T. E. Field, "A Data-Driven Global Sensitivity Analysis Framework for Three-Phase Distribution System With PVs," *IEEE Trans. Power Syst.*, vol. 36, no. 5, pp. 4809-4819. Sept. 2021, 10.1109/TPWRS.2021.3069009.

[17] D. L. H. Aik and G. Andersson, "Analysis of Voltage and Power Interactions in Multi-Infeed HVDC Systems," *IEEE Trans. Power Del.,* vol. 28, no. 2, pp. 816-824. Apr. 2013, 10.1109/TPWRD.2012.2227510.

[18] H. Xiao, X. Duan, Y. Zhang, and Y. Li, "Analytically Assessing the Effect of Strength on Temporary Overvoltage in Hybrid Multi-Infeed HVdc Systems," *IEEE Trans. Power Electron.*, vol. 37, no. 3, pp. 2480-2484. Mar. 2022, 10.1109/TPEL.2021.3112606.

[19] X. Chen, A. M. Gole, and M. Han, "Analysis of Mixed Inverter/Rectifier Multi-Infeed HVDC Systems," *IEEE Trans. Power Del.*, vol. 27, no. 3, pp. 1565-1573. Jul. 2012, 10.1109/TPWRD.2012.2187356.

[20] S. Cai, L. Shen, L. Jiang, Y. Tao, G. Qiu, and T. Wang, "Data-driven Critical Factor Identification for Sending-end Planning with Multi-outfeed HVDC," *iSPEC*, Nanjing, China, 2021, pp. 4004-4008.

[21] A. A. Girgis and W. L. Peterson, "Adaptive estimation of power system frequency deviation and its rate of change for calculating sudden power system overloads," *IEEE Trans. Power Del*., vol. 5, no. 2, pp. 585-594. Apr. 1990, 10.1109/61.53060.

[22] Y. Zheng, J. Li and Y. Jiao, "Distribution Network Planning and Comprehensive Investment Evaluation Based on Bayes-Entropy weight-Fuzzy Analytic Hierarchy Process," *IEEE International Conference on Power Electronics, Computer Applications (ICPECA),* Shenyang, China, 2021, pp. 477-481.

[23] Y Wind and T L Saaty. "Marketing applications of the analytic hierarchy process,". *Management science*, vol. 26, no. 7, 1980, pp. 641-658.

[24] A. S. Alghamdi, K. Polat, A. Alghoson, A. A. Alshdadi, and A. A. Abd El-Latif, "Gaussian process regression (GPR) based non-invasive continuous blood pressure prediction method from cuff oscillometric signals," *Appl Acoust,* vol. 164, p. 107256, Jul. 2020, 10.1016/j.apacoust.2020.107256

[25] I. M. Sobol, "Global sensitivity indices for nonlinear mathematical models and their Monte Carlo estimates," *Math Comput Simul,* Article vol. 55, no. 1-3, pp. 271-280. Feb. 2001, 10.1016/S0378-4754(00)00270-6.

[26] A. Saltelli, P. Annoni, I. Azzini, F. Campolongo, M. Ratto, and S. Tarantola, "Variance based sensitivity analysis of model output. Design and estimator for the total sensitivity index," *Comput Phys Commun,* vol. 181, no. 2, pp. 259-270, Feb. 2010, 10.1016/j.cpc.2009.09.018.

Li Shen State Grid Southwest Branch Corporation, State Grid Corporation of China, Chengdu, Sichuan. He is a senior engineer. He is engaged in power system production management and dispatching operation.

Li Jiang State Grid Southwest Branch Corporation, State Grid Corporation of China, Chengdu, Sichuan. He is a senior engineer. His research interests include power system grid planning.

Qiao Ming College of Electric Engineering, Sichuan University, Chengdu, China. She is currently pursuing the bachelor's degree in electrical engineering with Sichuan University, China. Her research interests include power system stability and control.

Qing Wang State Grid Southwest Branch Corporation, State Grid Corporation of China, Chengdu, Sichuan. He is a senior engineer. His research interests include ultra-high voltage DC transmission and flexible DC transmission.

Yiyu Wen State Grid Southwest Branch Corporation, State Grid Corporation of China, Chengdu, Sichuan. He is a senior engineer. His research interests include power system stability and control.